HHS Public Access

Author manuscript

Neuron. Author manuscript; available in PMC 2016 March 04.

Published in final edited form as:

Neuron. 2015 March 4; 85(5): 1132–1144. doi:10.1016/j.neuron.2015.01.017.

Implementation of linear sensory signaling via multiple coordinated mechanisms at central vestibular nerve synapses

Lauren E. McElvain[1,2,3], **Michael Faulstich**[2], **James M. Jeanne**[1], **Jeffrey D. Moore**[1], and **Sascha du Lac**[1,2,4,5]

[1]Neurosciences Graduate Program, University of California San Diego, 9500 Gilman Drive, La Jolla, CA 92093, USA

[2]Salk Institute for Biological Studies, 10010 N Torrey Pines Rd, La Jolla, CA 92037, USA

[3]Champalimaud Neuroscience Programme, Champalimaud Centre for the Unknown, Av. Brasília, Doca de Pedrouços, Lisbon 1400-038, Portugal

[4]Howard Hughes Medical Institute, 10010 N Torrey Pines Rd, La Jolla, CA 92037, USA

[5]Johns Hopkins University School of Medicine, 720 Rutland Avenue, Ross 420, Baltimore, MD 21205, USA

Summary

Signal transfer in neural circuits is dynamically modified by the recent history of neuronal activity. Short-term plasticity endows synapses with nonlinear transmission properties, yet synapses in sensory and motor circuits are capable of signaling linearly over a wide range of presynaptic firing rates. How do such synapses achieve rate-invariant transmission despite history-dependent nonlinearities? Here, ultrastructural, biophysical, and computational analyses demonstrate that concerted molecular, anatomical, and physiological refinements are required for central vestibular nerve synapses to linearly transmit rate-coded sensory signals. Vestibular synapses operate in a physiological regime of steady-state depression imposed by tonic firing. Rate-invariant transmission relies on brief presynaptic action potentials that delimit calcium influx, large pools of rapidly mobilized vesicles, multiple low-probability release sites, robust postsynaptic receptor sensitivity, and efficient transmitter clearance. Broadband linear synaptic filtering of head motion signals is thus achieved by coordinately tuned synaptic machinery that maintains physiological operation within inherent cell biological limitations.

Correspondence and requests for materials should be addressed to Dr. Sascha du Lac (sascha@jhmi.edu) or Dr. Lauren E. McElvain(lauren.mcelvain@neuro.fchampalimaud.org)..

Introduction

The efficacy of central synapses changes dynamically in response to activity, a process known as short-term synaptic plasticity (Zucker and Regehr, 2002). The specific characteristics of short-term plasticity vary substantially across different types of synapses, resulting in specialized signal transformations thought to subserve specific computations (Abbott and Regehr, 2004; Klug et al., 2012; Pfister et al., 2010). Extensive research has suggested that the mechanisms underlying short-term plasticity limit synapses in the central nervous system to inherently non-linear operation (Abbott and Regehr, 2004; Klug et al, 2012; Zucker and Regehr, 2002). Nonetheless, several synapses in sensory and motor circuits have recently been shown to operate in a linear regime in which synaptic strength remains constant despite variations in presynaptic activity (Arenz et al., 2008; Bagnall et al., 2008; Lorteije et al., 2009). By enabling postsynaptic firing to scale linearly with presynaptic firing (Bagnall et al., 2008), rate-invariant synapses mediate a fundamental computation in circuits that signal via rate codes.

Despite its computational simplicity, linear signaling poses a significant challenge for synaptic machinery. History-dependent mechanisms compromise linearity at each stage of synaptic transmission and include activity-dependent Ca2+ accumulation**,** vesicle depletion, neurotransmitter accumulation, and postsynaptic receptor desensitization (Fioravante and Regehr, 2011; Jones and Westbrook, 1996; Xu-Friedman and Regehr, 2004). Given the plethora of known cell biological constraints, what mechanisms enable synapses to signal with constant efficacy across a wide range of presynaptic firing rates? In principle, linear (rate-invariant) synaptic transmission could be implemented via any of several different strategies including mutually offset short-term depression and facilitation, one-to-one transmission via calyceal synaptic architecture, and specialized molecular components. From a functional perspective, however, the mechanistic implementation of signaling across any type of synapse must satisfy anatomical, computational, and behavioral requirements specific to each neural circuit.

The first central synapse in the vestibular system provides powerful functional and quantitative constraints for investigating how synaptic dynamics are tuned to meet behavioral demands. Primary sensory signals about head motion and gravity from the inner ear reach the central nervous system exclusively via vestibular nerve synapses (Angelaki and Cullen, 2008; Fernandez and Goldberg, 1971; Goldberg and Fernandez, 1971a). Unlike in the neighboring auditory system, where individual auditory nerve afferents encode a limited range of sound frequencies (Katusuki et al., 1958), vestibular nerve afferents each respond to the entire range of behaviorally relevant head movement frequencies and thus serve as wide bandwidth linear encoders of head velocity (Goldberg and Fernandez, 1971b; Fernandez and Goldberg, 1971). For vestibular behaviors to be generated accurately, rate-coded head motion signals must drive linear changes in firing rates of postsynaptic premotor neurons (Goldberg et el., 2012; Shimazu and Precht, 1965). To see clearly during self-motion, for example, compensatory eye movements should be linear functions of head motion, as is indeed the case for the vestibulo-ocular reflex (Bagnall et al., 2008; Robinson, 1981). Behavioral requirements thus provide stringent constraints on synaptic machinery: vestibular afferent synapses must operate linearly over the entire behaviorally relevant range

of head motion. In vitro analyses indicate that vestibular nerve synapses indeed exhibit wide-bandwidth, rate-invariant transmission, which mediates remarkably linear transformations from presynaptic to postsynaptic firing rates (Bagnall et al., 2008). The underlying synaptic architecture and mechanisms, however, remain unknown.

Here, we use electrophysiology, pharmacology, electron microscopy, and computational modeling to demonstrate that vestibular nerve synapses implement broadband linear filtering via the concerted expression of several anatomical and physiological components commonly observed at fast central synapses that do not exhibit linear filtering. By tuning each component of synaptic machinery for rapid, low gain operation and distributing synaptic load across multiple release sites, vestibular nerve synapses meet behavioral requirements for robust linear transmission of rate-coded signals. These results imply that a conserved toolbox of synaptic mechanisms can generate diverse transfer functions that are differentially tuned to meet specific circuit and behavioral demands and that nonlinear signaling at synapses in other circuits reflects computational specializations rather than history-dependent synaptic limitations.

Results

Sustained transmission at central vestibular nerve synapses is rate-invariant across the physiological operating range

In vivo, vestibular nerve afferents encode head velocity as broadband, linear modulations of firing rate (Fernandez and Goldberg, 1971; Goldberg and Fernandez, 1971b). We examined vestibular nerve synaptic transmission using whole-cell patch-clamp recordings of vestibular nucleus neurons in mouse brainstem slices in physiological extracellular Ca2+ (1.5mM). Trains of stimuli applied to the vestibular nerve elicited excitatory postsynaptic currents (EPSCs), previously shown to be mediated by α-amino-3-hydroxy-5-methyl-4-isoxazolepropionic acid (AMPA) receptors (McElvain et al., 2010), which exhibited short-term depression (Figure 1A, B) similar to recordings in supraphysiological extracellular Ca2+ (2.5 mM; Bagnall et al., 2008). Peak EPSC amplitude decreased over the initial 10-15 pulses to a sustained, steady-state level that did not vary with stimulus rate (56.8 ± 3.3% at 10 Hz and 58.8 ± 3.8% at 100 Hz; n = 11; p = 0.37; Figure 1B). Consequently, steady-state charge transfer across the synapse scaled linearly with stimulus rate over a wide range of frequencies, from 5-100 Hz (R^2 = 0.998, n = 11; Figure 1C).

In behaving animals, vestibular afferents fire tonically at high rates when the head is stationary (55 Hz on average in mice; Lasker et al., 2008), and head movements evoke bidirectional modulations around baseline firing rates. To determine physiologically relevant firing statistics of nerve afferents, we convolved gyroscopic measurements of head motion in behaving mice with published transfer functions from mouse vestibular afferents (Figure S1; Lasker et al., 2008). These analyses indicated that in freely running mice, the majority of vestibular afferents (>90%) maintain firing within the range of 5-100 Hz (Figure S1). Stimulation of the vestibular nerve *in vitro* with naturalistic afferent firing patterns evoked EPSCs that depressed rapidly to a sustained, steady-state amplitude which was maintained despite fluctuations in stimulus pattern and rate (Figure 1D). These findings indicate that

under behavioral conditions, vestibular nerve synapses operate in a steady-state regime of constant-amplitude depression.

Anatomical and quantal basis of transmission

Mechanisms of short-term depression at central synapses typically depend markedly on the rate and history of presynaptic activity (Zucker and Regehr, 2002). To determine how steady-state transmission at central vestibular synapses remains constant over a ~20-fold range of presynaptic firing rates, we first examined the underlying structural basis using electron microscopy (EM). Vestibular nerve afferents were labeled *in vivo* with fluorescent dextran conjugates, and afferent boutons were imaged by serial EM (see Experimental Procedures). Three-dimensional reconstructions revealed that boutons were exceptionally large, averaging 15.8 ± 4.7 μm^3 in volume, and contained 14 ± 6 distinct active zones (n = 8; Table S1; Figure 2A, B). Across the boutons, the average active zones ranged in size from 0.07 to 0.32 μm^2 and were separated by distances ranging between 0.13 and 0.86 μm (Table S1). Boutons contained over 12,000 vesicles, with several vesicles closely apposed to the presynaptic face of each active zone, and large vesicle pools that extended across multiple active zones. Vestibular afferent fibers contact single postsynaptic neurons via an average of 2-3 collaterals (Hauglie-Hanssen, 1968; Sato and Sasaki, 1993), suggesting the total number of release sites per connection could be relatively high. Although synapses that exhibit short-term depression typically have a high probability of neurotransmitter release (P_R), a large number of release sites could enable vestibular nerve synapses to operate effectively with a low P_R.

To test this hypothesis, we quantified the number of functionally independent release sites and their probability of neurotransmitter release using fluctuation analysis. EPSCs were elicited at low rates (0.067 or 0.2 Hz) and measured under 4 - 5 release probability conditions imposed by varying external Ca2+ and Mg2+ (Figure 3A). In contrast to many well-studied central synapses (Borst and Sakmann, 1996; Mintz et al., 1995; Schneggenburger and Neher, 2000; Schneggenburger and Neher, 2005), EPSC amplitude increased linearly with external Ca2+ from 0.75 – 4 mM (R^2 = 0.99; Figure 3B), similar to the linear Ca2+-dependence of release at the peripheral hair cell synapse onto vestibular nerve afferents (Dulon et al., 2009). The underlying quantal parameters were determined from the mean and variance of the peak EPSC amplitude using multiple-probability fluctuation analysis (MPFA), a multinomial model of release (Silver, 2003; Figure 3C; Experimental Procedures). MPFA estimated the total number of functional release sites per connection (N) to be 36 ± 6 (n = 9; Figure 3D). The mean quantal size (Q_P) for these connections was -28.4 ± 5.5 pA (Figure 3D), consistent with independent estimates from strontium-induced asynchronous release (-24.9 ± 2.0 pA, n = 5; p = 0.80). P_R scaled linearly with external Ca2+ and was 0.22 ± 0.04 in physiological Ca2+ (Figure 3D, E). These analyses indicate that head movement signals are transmitted to the central nervous system via synapses that exhibit a shallow, linear dependence on Ca2+ and whose operation depends on the aggregate function of multiple release sites with an intermediate-low initial P_R.

To assess the basis of short-term depression over the initial 10-15 pulses at vestibular nerve synapses, we paired MPFA with coefficient of variation (CV) analysis (Saviane and Silver, 2007) in 6 experiments (see Experimental Procedures). Using the MPFA estimates of the number of release sites, CV analysis tracked Q_P and P_R during stimulus trains in 1.5 mM Ca2+. Q_P did not change significantly over successive stimuli ($Pulse_1$: -16.5 ± 3.0 pA, $Pulses_{15-20}$: -20.5 ± 3.8 pA, p = 0.16), consistent with previous evidence that postsynaptic AMPARs neither desensitize nor saturate at vestibular nerve synapses (Bagnall et al., 2008). In contrast, P_R decreased with successive stimuli to 53.3 ± 5.5% of its initial value ($Pulse_1$ vs. $Pulses_{15-20}$, p = 0.03; Figure 3F). Thus, short-term depression at vestibular nerve synapses is mediated by an activity-dependent decrease in P_R from 0.22 to 0.12. Head motion signals thereby enter the central nervous system via synapses whose P_R is depressed such that of the 36 total release sites distributed across several boutons (Sato and Sasaki, 1993), only ~4 are predicted to release transmitter in response to an action potential.

Fast presynaptic action potential kinetics linearize transmission by restricting Ca influx to ensure low release probability

Short-term depression commonly occurs at high-P_R synapses due to use-dependent limitations in transmission machinery, such as vesicle depletion. To assess the basis of short term depression at vestibular nerve synapses, we examined the influence of manipulating initial P_R. Increasing Ca2+ from 1.5 to 2.5 mM nearly doubled P_R to 0.39 (Figure 3E) but had no effect on the magnitude of short-term depression (Figure 4A, B; 10 Hz, p=1.0; 100 Hz, p=0.88). In contrast, further increases in Ca2+ to 3.6 mM (P_R= 0.57) evoked significantly greater depression which depended on stimulus rate (Figure 4A, B; 10 Hz vs 100 Hz, p=0.03), consistent with activity-dependent depletion of synaptic vesicles or postsynaptic receptor desensitization at elevated P_R. The invariance of short-term depression to P_R at more physiological Ca2+ levels suggests that short-term depression at vestibular synapses reflects a regulatory mechanism rather than a resource-dependent biological limitation.

The relatively low P_R at vestibular nerve synapses under physiological conditions could result either from release machinery with intrinsically weak Ca2+ coupling or sensitivity or from restricted Ca2+ influx. Presynaptic Ca2+ influx is limited at many wide-bandwidth synapses by rapid action potential kinetics (Geiger and Jonas, 2000; Ishikawa et al., 2003; Sabatini and Regehr, 1997) imposed by fast-inactivating K channels (Gittis and du Lac, 2007; Rudy and McBain, 2001). To test whether rapid K currents limit Ca2+ influx and P_R, we blocked Kv3 and BK channels with 1mM TEA. Applying TEA increased peak EPSC amplitude to 265 ± 37% of baseline (n = 6, p = 0.03; Figure 4C, D) and increased steady-state EPSC amplitude at all stimulation rates (5 - 125 Hz; Figure 4E, F) but had no effect on the linear dependence of release on extracellular Ca2+ (Figure S2). Notably, the magnitude of short-term depression increased with stimulus rate in TEA (Figure 4E), thereby compromising linear synaptic charge transfer (Figure 4F). These results indicate that, consistent with observations at commonly studied synapses, vestibular nerve depression is rate-dependent under unphysiological conditions of high P_R. Under physiological conditions, however, by restricting Ca2+ influx to minimize P_R, rapid presynaptic K+ currents enable high-bandwidth transmission without rate-dependent decrements.

Vestibular nerve synapses have large vesicle pools and fast vesicle dynamics

To determine the transmission capacity of vestibular nerve vesicle pools, we quantified the number of vesicles per release site and their rate of reloading. Stimulation at 100 Hz for 1 minute resulted in occasional EPSC failures after 40 sec in 7 of 8 synapses (Figure 5A), indicating reserve vesicle pool depletion (Saviane and Silver, 2006a; Schneggenburger et al., 1999). In the absence of a reserve pool, the rate of vesicle refilling determines steady-state transmission and can be estimated from the cumulative EPSC slope (Figure 5B) and quantal amplitude (Figure 3D). This analysis indicated that refilling occurred at an average rate of 7.1 ± 1.7 vesicles/s per release site (n = 7). Back-extrapolation from the cumulative EPSC slope indicated that full reserve pools were exceptionally large, containing 233 ± 93 vesicles, consistent with EM observations (Figure 2). Given steady-state P_R of 0.12 (Figure 3), vesicle reloading is thus sufficiently fast to maintain full reserve pools at sustained firing rates < 60 Hz, which is remarkably well suited for dynamic encoding of head velocity signals in afferents which fire tonically at average rates of 55 Hz (Lasker et al., 2008).

In the presence of large vesicle pools, the speed at which reserve vesicles are readied for release limits transmission at high rates. To quantify this rate, we measured synaptic responses to intense bursts of stimuli. EPSCs evoked by 50 stimuli at 300 Hz exhibited stronger depression (25.9 ± 5.2 %) than EPSCs evoked at physiological rates (Figure 5C). This stronger depression recovered rapidly to the steady-state level evoked by 10 or 100 Hz trains (tau = 22 ms, n =12; Figure 5C, D). This recovery rate, which predominantly reflects the dynamics of vesicle translocation, docking, and priming, is comparable the fastest previously observed in the central nervous system (Hallermann et al., 2010; Saviane and Silver, 2006a). Notably, the rapid recovery from releasable vesicle depletion is segregated temporally by ~500 ms from the recovery from steady-state depression to baseline, which reflects the restoration of P_R to pre-stimulation levels (Figure 5D). Although many synapses express plasticity with fast (10s ms), intermediate (100s ms), and slow (sec) recovery kinetics (Dittman and Regehr, 1998; Varela et al., 1997; Zucker and Regehr, 2002), vestibular nerve synapses are devoid of dynamic mechanisms that change over intermediate timescales. Taken together, these results demonstrate that although vestibular nerve synapses have large pools of vesicles with dynamics that are among the fastest in the central nervous system, vesicle translocation speed is not sufficient to sustain broadband (5-100 Hz) rate-invariant transmission in the absence of a low P_R (Figure 4A, B).

Temporal precision at high rates depends on active glutamate uptake

To subserve behavior, vestibular nerve transmission must meet significant temporal challenges: vestibulo-motor reflexes occur with latencies as short as 7 ms (Huterer and Cullen, 2002) and are sensitive to rapid changes in head movement. The rapid kinetics of EPSCs and lack of effect of γ-DGG (Wong et al., 2003) on short-term depression under normal and elevated P_R conditions (Figure S3) are consistent with previous observations that AMPARs at vestibular nerve synapses neither desensitize nor saturate (Bagnall et al, 2008) and further suggest that release sites operate independently, without significant glutamate spillover or accumulation. To determine whether passive or active clearance restricts glutamate diffusion and accumulation, we blocked glutamate transporters (EAAT1-5) with dl-TBOA (200 μM)(Shimamoto et al., 1998). Under control conditions, EPSC responses are

phasic and summation is minimal at vestibular nerve synapses, however train stimulation in dl-TBOA evoked an accumulating, tonic current that persisted for several seconds following the cessation of stimulation (Figure 6A). dl-TBOA did not alter the kinetics of phasic EPSCs (fall time, 90-10%: 3.5 ± 0.6 ms baseline; 3.5 ± 0.6 ms TBOA; p= 0.81). Rate-invariant depression of phasic EPSCs was also unaffected by dl-TBOA (Figure 6B). However, evoked postsynaptic firing was no longer proportional to presynaptic firing; instead, postsynaptic responses mimicked the behavior of a leaky integrator, increasing during steady stimulation and decaying slowly after stimulus offset (Figure 6C, D). Thus, glutamate transporters are not required for rate-invariance per se but play a fundamental role in constraining linearity to behaviorally relevant timescales. In combination with rapid AMPAR kinetics and minimal NMDAR currents (Bagnall et al., 2008; McElvain et al., 2010), efficient transporters specialize vestibular nerve synapses for short-latency, linear transmission of sensory information.

Computational model of synaptic transmission

To determine whether these findings can account quantitatively for the dynamics and high-bandwidth linearity of vestibular nerve synapses, we constructed a model of synaptic transmission constrained by our experimental results (Figure 7A, see Experimental Procedures). MPFA and CV analyses determined the number of release site (N), the initial P_R, and the activity-dependent regulation of P_R (Figure 3); depletion and recovery experiments determined vesicle pool size and dynamics, as well as the time course of P_R recovery (Figure 5). Postsynaptic sensitivity was constant (Figure S3; Bagnall et al., 2008), and release sites operated independently, without spillover or accumulation (Figure 6). Vesicles at each release site transitioned with Poisson statistics from a reserve pool to a release-ready state, and the single free parameter, the number of docked vesicles, was set to 2 (see Experimental Procedures). In response to stimulus trains, this simple model exhibited synaptic dynamics that matched experimentally observed results. Model EPSCs depressed over the initial 10 stimuli to a steady-state level that was independent of stimulus rate between 5 and 100 Hz but varied with rates above and below this physiologically relevant range (Figure 7B, C). The model successfully captured the experimentally observed magnitude of steady-state depression and range of rate-invariance (Figure 7C), as well as the corresponding linear charge transfer (Figure 7D).

In vivo, vestibular afferents rarely cease firing (Figure S1), implying that synaptic transmission operates in a steady-state regime of rate-invariance. We probed the model with stimuli derived from head velocity measurements in freely running mice, as tested experimentally in Figure 1D. In response to these naturalistic stimuli, model EPSCs depressed rapidly to a steady-state level that was maintained indefinitely despite time-varying fluctuations in input rate (Figure 7E). Thus, a simple model, constrained by experimental results, accounts for the ability of vestibular nerve synapses to encode head movements linearly in the face of tonic presynaptic firing.

We probed the model to examine the dependence of short-term plasticity on several synaptic properties. The upper bound on rate-independence was constrained by P_R and vesicle dynamics. Model output depended steeply on rate when initial P_R was increased to 0.64

(Figure 8A, D), similar to experimental observations (Figure 4A, B). This rate-dependence resulted from depletion of readily-releasable vesicles, which also occurred in response to supra-physiological activity (300 Hz) (Figures 5C, 7C). The lower bound on linearity depended on the timecourse of recovery from P_R depression. Under physiological conditions, recovery opposed short-term depression at rates < 5 Hz, but was sufficiently slow to saturate and not influence transmission at rates > 5 Hz (Figure 7B). Advancing the timecourse of recovery by 500 ms reduced the range of rate-invariant transmission due to the opposition of recovery and depression at low rates (Figure 8B, D). Synaptic variability, but not linearity, depended on the number of release sites (Figure 8C, D). Together with experimental results, these findings indicate that several synaptic properties must be appropriately tuned for vestibular synapses to implement reliable rate-invariant transmission across the broad physiological range of presynaptic firing rates, including the number of release sites, the regulation of Ca2+ influx, vesicle pool size and dynamics, the dynamics of P_R depression and recovery, glutamate uptake, and the kinetics and sensitivity of postsynaptic glutamate receptors.

Discussion

This study demonstrates that vestibular nerve synapses transform dynamic, rate-coded sensory signals into linear modulations of postsynaptic firing via the coordinated tuning of several distinct anatomical and physiological components. Presynaptic terminals comprising multiple release sites employ rapid action potentials to delimit Ca2+ influx and P_R, while high temporal fidelity of signal transfer is conferred by efficient glutamate clearance and independent activation of postsynaptic receptors with fast kinetics. Steady-state conditions of tonic presynaptic firing drive sustained reductions in P_R that prevent vesicle supply rundown during high-rate transmission. The fundamental computation performed by vestibular nerve synapses—wide-bandwidth linear filtering—could be produced, in principle, by overpowering calyceal synapses that ensure robust 1:1 postsynaptic responses to each presynaptic action potential. This arrangement, however, would preclude two critical operations of vestibular circuits: multisensory integration (Angelaki and Cullen, 2008; Sadeghi et al., 2012) and long-term, bidirectional experience dependent plasticity (McElvain et al., 2010; Menzies et al., 2010, Scarduzio et al., 2012). By distributing synaptic load across multiple independent release sites and operating well within the inherent dynamic limitations of cell biological machinery, vestibular nerve synapses satisfy systems requirements for wide bandwidth linear encoding, postsynaptic signal integration, and adaptive gain control.

Sustained high-rate synaptic transmission

Operating reliably in a regime of maintained high firing rates poses significant challenges for synaptic machinery. The extreme rapidity of vestibular reflexes, which can exhibit latencies < 7 ms (Huterer and Cullen, 2002), requires afferents to respond quickly and robustly to head motion despite firing at spontaneous rates that exceed the maximum capacity of many classes of central neurons. Several mechanistic implementations that promote adequate vesicle availability at vestibular synapses have been observed in other fast-firing neurons in the cerebral cortex, hippocampus, cerebellum, and brainstem (Crowley

et al., 2007; Hallermann and Silver, 2013; Hu et al., 2014). Rapid repolarization of presynaptic action potentials by Kv3 currents (Gittis et al., 2010; Kolkman et al., 2011; Rudy and McBain, 2001) minimizes Ca2+ influx and reduces P_R (Geiger and Jonas, 2000; Ritzau-Jost et al., 2014; Sabatini and Regehr, 1997; Taschenberger and von Gersdorff, 2000; Telgkamp et al., 2004). Large vesicle pools, multiple release sites, and rapid kinetics of vesicle translocation, docking, and priming maintain vesicle availability during high-rate transmission. Notably, the dynamics of vesicle mobilization at vestibular nerve synapses (Figure 5) are comparable to the fastest previously described in the central nervous system, at cerebellar mossy fiber synapses (Hallermann et al., 2010; Saviane and Silver, 2006a), suggesting that conserved mechanisms of vesicle mobility (Hallermann and Silver, 2013) may set an upper bound on the rate of vesicle availability at central synapses.

Rate-invariant transmitter release and presynaptic calcium dynamics

At many central synapses, facilitation and depression occur simultaneously, and synaptic filtering is dominated by the relative balance of these opposing short-term mechanisms (Zucker and Regehr, 2002). As such, it has been assumed that rate-invariant transmission is conferred by depression and facilitation which are mutually offset (Fortune and Rose, 2001; Klyachko and Stevens, 2006). Vestibular synapses, however, appear devoid of any offsetting facilitation: the magnitude of depression evoked by physiological activity does not depend on either presynaptic firing rate or pattern and is invariant to variations in extracellular Ca2+ levels (Figure 4B). History-dependent presynaptic Ca2+ accumulation, a common basis of short-term facilitation, might be significantly limited at vestibular synapses by a combination of properties shared by fast-firing inhibitory interneurons in the forebrain (Hu et al., 2014), which include restricted Ca2+ influx via P/Q-type channels, efficient buffering by parvalbumin, and a nanodomain arrangement of Ca2+ channels and release sites. Transmission at vestibular nerve synapses is mediated entirely by P/Q-type channels (Figure S4), which are tightly coupled to exocytotic machinery (Bucurenciu et al., 2010; Bucurenciu et al., 2008; Eggermann et al., 2012; Eggermann and Jonas, 2012; Hefft and Jonas, 2005; Kim et al., 2013) and can limit the Ca2+ cooperativity of release (Fedchyshyn and Wang, 2005; Mintz et al., 1995). Vestibular ganglion cells express high levels of parvalbumin (Eatock and Songer, 2011; Kevetter, 1996; Raymond et al., 1993), which can impose Ca2+ nanodomains and preclude short-term facilitation (Eggermann and Jonas, 2012). The insensitivity of vestibular nerve transmission to prolonged application of membrane permeable Ca2+ buffers EGTAAM (Bagnall et al., 2008) and BAPTA-AM (Figure S4) is additionally consistent with efficient presynaptic Ca2+ buffering.

Although the relationship between presynaptic Ca2+ concentration and transmitter release is highly cooperative at many central synapses (Schneggenburger and Neher, 2005), release scales linearly with external Ca2+ at vestibular nerve synapses (Figure 3). A near-linear dependence of release on extracellular Ca2+ has also been observed at central olfactory nerve synapses (Murphy et al., 2004). The relationship between Ca2+ influx and transmitter release can be influenced by several factors beyond the inherent cooperativity of presynaptic Ca2+ sensors, including the recruitment of readily releasable vesicles (Thanawala and Regehr, 2013), Ca2+ buffering capacity (Fedchyshyn and Wang, 2005; Kochubey et al, 2009), and the type and location of Ca2+ channels (Matveev et al., 2011). At peripheral

synapses where release depends linearly on Ca2+, tight coupling of small numbers of Ca2+ channels to release machinery and nanodomain restriction of Ca2+ results in rapid saturation of cooperative Ca2+ sensors (Beutner and Moser, 2001; Brandt et al., 2005; Goutman and Glowatzki, 2007; Johnson et al., 2010; Keen and Hudspeth, 2006). A similar nanodomain coupling of a non-linear Ca2+ sensor under tight regulation by parvalbumin (Eggerman and Jonas, 2012) could account for the relationship between external Ca2+ and release at vestibular nerve synapses.

Signal fidelity requires rapid, independent activation of postsynaptic receptors

At many synapses, the maintenance of transmission at high rates relies on spillover, in which individual postsynaptic receptors are contacted by neurotransmitter from multiple presynaptic release sites (DiGregorio et al., 2002; Meyer et al., 2001; Telgkamp et al., 2004; von Gersdorff and Borst, 2002). Vestibular nerve synapses, however, appear to independently influence restricted populations of postsynaptic receptors (Figure S3; Bagnall et al., 2008). From a functional perspective, the reductions in temporal fidelity that accompany spillover would be deleterious for the exceptionally short latency and rapid response dynamics of vestibulo-motor behaviors. Active transmitter clearance is indeed critical for short-latency synaptic linearity; in the absence of glutamate transporters, vestibular synaptic transmission is transformed from broadband filtering to leaky integration (Figure 6).

AMPARs at vestibular nerve synapses are remarkably resistant to desensitization even under conditions of high P_R (Figure S3) or glutamate pooling (Figure 6B). This robust and maintained sensitivity of postsynaptic AMPARs is likely conferred by the composition of subunit isoforms and/or auxiliary proteins (Mosbacher et al., 1994; Nicoll et al., 2006; Partin et al., 1996; Priel et al., 2005). Transmission at vestibular nerve synapses is mediated by AMPARs with rapid kinetics, including Ca2+-permeable AMPARs, and a limited NMDAR contribution (McElvain et al., 2010), which are well suited for short-latency signaling. In contrast to circuits that integrate signals over hundreds of milliseconds to seconds, the rapidity of vestibular reflexes necessitates tight temporal control and short-latency signal transfer. The unusual combination of rate-invariant release, active transmitter clearance, and independent activation of rapid, constant-sensitivity postsynaptic receptors make the vestibular nerve synapse a particularly tractable model for examining the functional consequences of molecular manipulations of synaptic machinery.

Synaptic dynamics and the physiological operating range

In several intensively studied circuits, synapses with low initial P_R exhibit short-term facilitation, while those with high initial P_R exhibit depression (Zucker and Regehr, 2002). In contrast, vestibular nerve synapses exhibit depression despite a relatively low initial P_R, and the magnitude of depression remains constant across experimental alterations in P_R. A similar decoupling of initial P_R and short-term plasticity has been previously observed (Hefft et al, 2002; Kraushaar and Jonas, 2000). The reductions in P_R evoked at the onset of synaptic activity in vestibular afferents could reflect modifications of the intrinsic release properties of vesicles (Wu and Borst, 1999) or an alternative mechanism regulated by prolonged periods of inactivity. The reductions in P_R saturate quickly and recover slowly

relative to the maximum interspike interval experienced by most vestibular afferents (Figures S1, 5). As a consequence, rather than dynamically contributing to synaptic filtering, depression at vestibular synapses extends the range of rate-invariant transmission by limiting tonic release rates (Figure 8). In contrast, at cerebellar mossy fiber and Purkinje cell synapses, the temporal dynamics of short-term depression overlap with physiological interspike intervals (Saviane and Silver, 2006a; Telgkamp et el., 2004), thereby influencing synaptic computations under behaviorally relevant conditions.

Relevance for other synapses and systems

Given typical observations at popularly studied synapses in which history-dependent nonlinearities dominate short-term dynamics, the broadband linear filtering implemented by vestibular nerve synapses appears highly unusual. From a systems perspective, however, linear rate coding of sensory and motor signals has long been recognized as a hallmark of neurons throughout the vestibular, oculomotor, and skeletomotor systems (e.g. Fuchs and Luschei, 1970; Hobson and Scheibel, 1980; Larson et al., 1983; Lisberger and Fuchs, 1978a, b). Rather than utilizing uniquely specialized mechanisms, vestibular nerve synapses achieve rate-invariant transmitter release via presynaptic machinery conserved across high-rate synapses throughout the neuraxis (Hu et al., 2014; Lorteje et al., 2009; Teglkamp et al., 2004; Hallermann and Silver, 2013). By optimizing each stage of synaptic transmission for speed and brevity and distributing synaptic load across multiple low P_R release sites, vestibular nerve synapses employ a classic engineering solution for constructing a robust linear signaling device from nonlinear components (Black, 1934). This simple strategy has the additional benefit of being highly scalable, as is required to account for the diverse operating ranges of synapses in different systems and species. Increasing the number of release sites and decreasing P_R in our model, for example, could account for the remarkable transmission capacity of primate vestibular nerve afferents, which fire spontaneously at average rates of ~100 Hz (Goldberg and Fernandez, 1971a; Fernandez and Goldberg, 1971). By taking advantage of the tight functional constraints on synapses responsible for conveying rate-coded head motion signals to the central nervous system, this study demonstrates that within the physiological operating range, synaptic filtering properties can be tuned precisely to meet specific behavioral demands. The implementation of synaptic computations via multiple tuned cellular mechanisms implies that many subtle molecular perturbations could severely dysregulate synaptic computations required for behavioral performance, perception, and cognition.

Experimental Procedures

All experiments were carried out in accordance with the standards of the Salk Institute IACUC. Oblique coronal brainstem slices (300-μm) were prepared from P18-28 C57BL/6 mice as described previously (McElvain et al., 2010). The external recording solution contained (in mM): 124 NaCl, 5 KCl, 1.0 $MgSO_4$, 26 $NaHCO_3$, 1.5 $CaCl_2$, 1 NaH_2PO_4, and 11 dextrose and was bubbled with 95% O_2/5% CO_2. Recordings were made at 33-34 °C from medial vestibular nucleus neurons in the presence of 1-10 μM strychnine and 100 μM picrotoxin. EPSCs were measured at -75 mV, a potential at which vestibular nerve transmission is AMPAR-mediated (McElvain et al., 2010). Patch pipettes (2-5 MΩ) were

pulled from flame-polished glass and filled with solution containing (in mM): 140 K gluconate, 20 HEPES, 8 NaCl, 0.1 EGTA, 2 Mg-ATP, 0.3 Na_2-GTP, and 0.1 Spermine. EPSCs were quantified as the difference between the peak inward current and the average current 0.5 ms prior to each stimulus. The vestibular nerve was stimulated with 100-μs, biphasic pulses, delivered by a bipolar, concentric electrode (FHC) placed in the nerve fiber tract, lateral to the vestibular complex. Series resistance was monitored continuously, and recordings with a series resistance >16 MΩ were excluded. Data were acquired with a Multiclamp 700B, low-pass filtered at 4-10 kHz for voltage clamp and 10 kHz for current clamp, and digitized at 40 kHz with an ITC-18. House-written code in Igor 6 was used for acquisition. Data are reported as mean ± SEM, and statistical significance was evaluated with paired (where possible) or unpaired Wilcoxon signed-rank tests in KaleidaGraph 3.6. All chemicals were purchased from Sigma, Tocris, or Ascent Scientific.

Vestibular nerve labeling and EM analysis

Mice were deeply anesthetized with Ketamine/Xylazine (80 mg/kg and 10 mg/kg). The skull overlaying the cerebellum was exposed, and the interparietal plate was removed lateral to the midline. The portion of the lateral cerebellum overlaying the eighth nerve was then carefully aspirated, avoiding major blood vessels, until the nerve was exposed. Using a capillary glass pipette, a near-saturating solution of Texas red dextran (10,000 MW) in DI water was injected into the nerve where it exits the temporal bone. The exposed cavity was then filled with gelfoam soaked with lactated Ringer's, while the animal was kept anesthetized for 4-6 hours.

Mice were then anesthetized with Nembutal and transcardially perfused with PBS followed by 4% formaldehyde, 0.02% glutaraldehyde in PBS. The brain was removed and left in fixative until slicing. The brain was rinsed in cold PBS and cut into 50 μm slices on a vibratome. Slices were placed in a chamber and imaged on a fluorescence microscope to locate labeled vestibular nerve axons. Following imaging, slices were fixed in 2% glutaraldehyde in 0.1 M sodium cacodylate buffer, rinsed, postfixed in 1% osmium tetroxide and 1% potassium ferrocyanide, rinsed, en bloc stained in 1% uranyl acetate, dehydrated with glycol methacrylate and flat embedded in Epon. The slices were blocked and mounted onto Epon stubs for sectioning parallel to the plane of imaging. Ultrathin sections (~60 nm) were cut on an ultramicrotome, collected onto formvar-coated slot grids and stained with 2% uranyl acetate and 0.2% lead citrate. The sections were examined in a JEOL 100CXII transmission electron microscope equipped with a digital camera. Axons identified by EM were matched to the fluorescent images on the basis of morphology and location. Images of vestibular boutons were manually aligned via rotations and translations so that membrane specializations and mitochondria were superimposable in serial sections. Boutons were traced, reconstructed, and analyzed using Reconstruct software (Fiala, 2005). Release sites were identified in each section based on a presynaptic cluster of vesicles apposed to a postsynaptic density. Release site segments were considered to belong to a single, continuous site when any portion was superimposable in serial images.

Estimation of quantal parameters

EPSCs were recorded at 0.067 or 0.2 Hz under 4-5 different extracellular Ca2+ concentrations (0.5 – 4mM), while the total divalent concentration (4.2 mM) was maintained by varying Mg2+. Stable epochs (80 ± 6 EPSCs per condition) were delimited by Spearman rank-order analysis, and quantal parameters were estimated using multiple probability fluctuation analysis (MPFA; Silver, 2003). Analyses were performed using custom-written MATLAB code. The relationship between the mean (I) and the variance of the peak EPSC amplitude (σ^2) at each synapse was approximated by the function:

$$\sigma^2(I) = \left\{ IQ_p\sigma \frac{Q_P \boldsymbol{I}^2 (1+\sigma)}{\boldsymbol{I} + NQ_P\sigma} \right\} \left(1 + CV_{QII}^2\right) + Q_P I CV_{QI}^2 \quad (1)$$

where Q_P is the quantal size, N is the number of release sites, CV_{QI} is the coefficient of variation of the intrasite quantal variability, CV_{QII} is the coefficient of variation of the intersite quantal variability, and α is a measure of the nonuniformity of release probability across release sites (Silver, 2003). The total quantal variation (0.56 ± 0.08; n=5) was measured from asynchronous EPSCs evoked in Sr2+ (5 mM). Inter- and intrasite variability were assumed to contribute equally to the total variability (Clements, 2003).

Data were fit to equation (1) using nonlinear least-squares regression. Errors in estimates of the variance were determined using h-statistics. Fits were evaluated using the chi-square goodness-of-fit test (Saviane and Silver, 2006b; Silver, 2003), and only fits with $p \geq 0.05$ were accepted for further analysis. Three experiments were rejected due to the maximal $P_R < 0.5$; one experiment was excluded because its mean-variance relationship was best modeled by a linear rather than a quadratic relationship.

Estimates of the number of release sites (N) and the quantal size (Q_P) were computed from equation (1). Estimates of P_R were then computed from the binomial model:

$$\boldsymbol{I} = NP_R Q_P. \quad (2)$$

Changes in quantal parameters during train stimulation were estimated using coefficient of variation (CV) analysis (Saviane and Silver, 2006b; Saviane and Silver, 2007). The CV of EPSC amplitude was calculated for each pulse in a 10 Hz train. Using the N from MFPA, P R was estimated using:

$$CV = \frac{\sigma}{\boldsymbol{I}} = \sqrt{\frac{(1 - P_R)\left(1 + CV_{QII}^2\right) + CV_{QI}^2}{NP_R}}. \quad (3)$$

Q_P was then calculated using equation (2). During train stimulation, transmission rapidly reaches steady-state, and the average EPSC from pulses 11-20 does not differ from pulses 30-50 ($p = 0.51$, 10 Hz). CV estimates from 20-pulse trains thus should adequately estimate steady-state parameters.

Models of dynamic synaptic transmission

Short-term plasticity at vestibular nerve synapses was modeled with a two-pool system of vesicle dynamics. At each of N release sites, vesicles transitioned from the reserve pool to the readily-releasable pool (RRP) with Poisson statistics, such that the probability that k vesicles transition to the RRP within a time interval dt has the distribution:

$$P_{\text{Reserve}\rightarrow RRP}(k) = \frac{\left(\frac{dt}{T_{RRP}}\right)^{k} e^{-\left(\frac{dt}{T_{RRP}}\right)}}{k!} \quad (4)$$

where τ_{RRP} is the time constant of transition to the RRP. All release sites were considered to be statistically independent of each other.

In response to an action potential, a RRP vesicle is released with probability Pr(t). Each action potential releases a maximum of one vesicle per release site. The release probability of each vesicle is a function of recent activity. Upon initial transition to the RRP, the release probability of each vesicle is set to the steady-state value, Pr. Based on the time course of depression recovery (Figure 5D), the release probability is constant unless more than 500 ms elapses since the last action potential. After 500 ms, release probability increases according to the differential equation:

$$\frac{dPr(t)}{dt} = -T_{\text{prime}}\left(Pr(t) - Pr_{Max}\right) \quad (5)$$

such that Pr(t) increases asymptotically to Pr_{Max} with a time constant of τprime. In its initial state, the release probability of each vesicle is set to Pr_{Max} to reflect the lack of nerve activity in the *in vitro* preparation.

Model parameters were based on experimental findings. From MPFA, Pr_{Max} was set to 0.22 and N (the total number of functional release sites) to 36. The steady-state release probability, Pr, was set to 0.12 based on CV analysis. Time constant τ_{RRP} was 22 ms, based on the kinetics of recovery from enhanced depression, and τprime was 2.67 s, the time constant of recovery from steady-state depression (Figure 5). Model linearity was confirmed by a ratio ≥ 0.96 of steady-state responses at 100 Hz vs. 10 Hz. The single free parameter was the maximum number of vesicles in the RRP. To optimize model function, this was set to two vesicles, which were docked and released in series. A model in which the RRP contained a single vesicle was linear if τ_{RRP} was reduced to 7.48 ms, but this one-vesicle model poorly predicted the rundown of transmission at high rates or under high-probability conditions. In contrast, the two-vesicle model captured these properties.

Supplementary Material

Refer to Web version on PubMed Central for supplementary material.

Acknowledgments

This work was supported by the National Eye Institute (RO1 EY11027) and the Howard Hughes Medical Institute. We thank Richard Jacobs for electron microscopy and Dr. Rui Costa for helpful comments on the manuscript.

References

Abbott LF, Regehr WG. Synaptic computation. Nature. 2004; 431:796–803. [PubMed: 15483601]

Angelaki DE, Cullen KE. Vestibular system: the many facets of a multimodal sense. Annu Rev Neurosci. 2008; 31:125–150. [PubMed: 18338968]

Arenz A, Silver RA, Schaefer AT, Margrie TW. The contribution of single synapses to sensory representation in vivo. Science. 2008; 321:977–980. [PubMed: 18703744]

Bagnall MW, McElvain LE, Faulstich M, du Lac S. Frequency-independent synaptic transmission supports a linear vestibular behavior. Neuron. 2008; 60:343–352. [PubMed: 18957225]

Beutner D, Moser T. The presynaptic function of mouse cochlear inner hair cells during development of hearing. J Neurosci. 2001; 21:4593–4599. [PubMed: 11425887]

Black HS. Stabilized feed-back amplifiers. American Institute of Electrical Engineers, Transactions of the. 1934; 53:114–120.

Borst JG, Sakmann B. Calcium influx and transmitter release in a fast CNS synapse. Nature. 1996; 383:431–434. [PubMed: 8837774]

Brandt A, Khimich D, Moser T. Few CaV1.3 channels regulate the exocytosis of a synaptic vesicle at the hair cell ribbon synapse. J Neurosci. 2005; 25:11577–11585. [PubMed: 16354915]

Bucurenciu I, Kulik A, Schwaller B, Frotscher M, Jonas P. Nanodomain Coupling between Ca2+ Channels and Ca2+ Sensors Promotes Fast and Efficient Transmitter Release at a Cortical GABAergic Synapse. Neuron. 2008; 57:536–545. [PubMed: 18304483]

Bucurenciu I, Bischofberger J, Jonas P. A small number of open Ca2+ channels trigger transmitter release at a central GABAergic synapse. Nat. Neurosci. 2010; 13:19–21. [PubMed: 20010820]

Clements JD. Variance-mean analysis: a simple and reliable approach for investigating synaptic transmission and modulation. J Neurosci Methods. 2003; 130:115–125. [PubMed: 14667541]

Crowley JJ, Carter AG, Regehr WG. Fast vesicle replenishment and rapid recovery from desensitization at a single synaptic release site. J Neurosci. 2007; 27:5448–5460. [PubMed: 17507567]

DiGregorio DA, Nusser Z, Silver RA. Spillover of glutamate onto synaptic AMPA receptors enhances fast transmission at a cerebellar synapse. Neuron. 2002; 35:521–533. [PubMed: 12165473]

Dittman JS, Regehr WG. Calcium dependence and recovery kinetics of presynaptic depression at the climbing fiber to Purkinje cell synapse. J Neurosci. 1998; 18:6147–6162. [PubMed: 9698309]

Dulon D, Safieddine S, Jones SM, Petit C. Otoferlin is critical for a highly sensitive and linear calcium-dependent exocytosis at vestibular hair cell ribbon synapses. J Neurosci. 2009; 29:10474–10487. [PubMed: 19710301]

Eatock RA, Songer JE. Vestibular hair cells and afferents: two channels for head motion signals. Annu Rev Neurosci. 2011; 34:501–534. [PubMed: 21469959]

Eggermann E, Bucurenciu I, Goswami SP, Jonas P. Nanodomain coupling between Ca(2)(+) channels and sensors of exocytosis at fast mammalian synapses. Nat Rev Neurosci. 2012; 13:7–21. [PubMed: 22183436]

Eggermann E, Jonas P. How the ‘slow’ Ca(2+) buffer parvalbumin affects transmitter release in nanodomain-coupling regimes. Nat Neurosci. 2012; 15:20–22. [PubMed: 22138646]

Fedchyshyn MJ, Wang LY. Developmental transformation of the release modality at the calyx of Held synapse. J Neurosci. 2005; 25:4131–4140. [PubMed: 15843616]

Fernandez C, Goldberg JM. Physiology of peripheral neurons innervating semicircular canals of the squirrel monkey. II. Response to sinusoidal stimulation and dynamics of peripheral vestibular system. J Neurophysiol. 1971; 34:661–675. [PubMed: 5000363]

Fiala JC. Reconstruct: a free editor for serial section microscopy. J Microsc. 2005; 218:52–61. [PubMed: 15817063]

Fioravante D, Regehr WG. Short-term forms of presynaptic plasticity. Curr Opin Neurobiol. 2011; 21:269–274. [PubMed: 21353526]

Fortune ES, Rose GJ. Short-term synaptic plasticity as a temporal filter. Trends Neurosci. 2001; 24:381–385. [PubMed: 11410267]

Fuchs AF, Luschei ES. Firing patterns of abducens neurons of alert monkeys in relationship to horizontal eye movement. J Neurophysiol. 1970; 33:382–392. [PubMed: 4985724]

Geiger JR, Jonas P. Dynamic control of presynaptic Ca(2+) inflow by fast-inactivating K(+) channels in hippocampal mossy fiber boutons. Neuron. 2000; 28:927–939. [PubMed: 11163277]

Gittis AH, du Lac S. Firing properties of GABAergic versus non-GABAergic vestibular nucleus neurons conferred by a differential balance of potassium currents. J Neurophysiol. 2007; 97:3986–3996. [PubMed: 17392422]

Gittis AH, Moghadam S, du Lac S. Mechanisms of sustained high firing rates in two classes of vestibular nucleus neurons: differential contributions of resurgent Na, Kv3, and BK currents. J Neurophysiol. 2010 in press.

Goldberg, JM.; Wilson, VJ.; Cullen, KE.; Angelaki, DE.; Broussard, DM.; Buttner-Ennever, J.; Fukushima, K.; Minor, LB. The Vestibular System: A Sixth Sense. Oxford University Press; 2012.

Goldberg JM, Fernandez C. Physiology of peripheral neurons innervating semicircular canals of the squirrel monkey. 3. Variations among units in their discharge properties. J Neurophysiol. 1971a; 34:676–684. [PubMed: 5000364]

Goldberg JM, Fernandez C. Physiology of peripheral neurons innervating semicircular canals of the squirrel monkey. I. Resting discharge and response to constant angular accelerations. J Neurophysiol. 1971b; 34:635–660. [PubMed: 5000362]

Goutman JD, Glowatzki E. Time course and calcium dependence of transmitter release at a single ribbon synapse. Proc Natl Acad Sci U S A. 2007; 104:16341–16346. [PubMed: 17911259]

Hallermann S, Fejtova A, Schmidt H, Weyhersmuller A, Silver RA, Gundelfinger ED, Eilers J. Bassoon speeds vesicle reloading at a central excitatory synapse. Neuron. 2010; 68:710–723. [PubMed: 21092860]

Hallermann S, Silver RA. Sustaining rapid vesicular release at active zones: potential roles for vesicle tethering. Trends Neurosci. 2013; 36:185–194. [PubMed: 23164531]

Hauglie-Hanssen E. Intrinsic neuronal organization of the vestibular nuclear complex in the cat. A Golgi study. Ergeb Anat Entwicklungsgesch. 1968; 40:3–105. [PubMed: 4178473]

Hefft S, Kraushaar U, Geiger JRP, Jonas P. Presynaptic short-term depression is maintained during regulation of transmitter release at a GABAergic synapse in rat hippocampus. J. Physiol. 2002; 539:201–208. [PubMed: 11850513]

Hefft S, Jonas P. Asynchronous GABA release generates long-lasting inhibition at a hippocampal interneuron-principal neuron synapse. Nat Neurosci. 2005; 8:1319–1328. [PubMed: 16158066]

Hermann J, Pecka M, von Gersdorff H, Grothe B, Klug A. Synaptic transmission at the calyx of Held under in vivo like activity levels. J Neurophysiol. 2007; 98:807–820. [PubMed: 17507501]

Hobson JA, Scheibel AB. The brainstem core: sensorimotor integration and behavioral state control. Neurosci Res Program Bull. 1980; 18:1–173. [PubMed: 7374965]

Hsu SF, Augustine GJ, Jackson MB. Adaptation of Ca(2+)-triggered exocytosis in presynaptic terminals. Neuron. 1996; 17:501–512. [PubMed: 8816713]

Hu H, Gan J, Jonas P. Interneurons. Fast-spiking, parvalbumin+ GABAergic interneurons: from cellular design to microcircuit function. Science. 2014; 345:1255263. [PubMed: 25082707]

Huterer M, Cullen KE. Vestibuloocular reflex dynamics during high-frequency and high-acceleration rotations of the head on body in rhesus monkey. J. Neurophysiol. 2002; 88:13–28. [PubMed: 12091529]

Ishikawa T, Nakamura Y, Saitoh N, Li WB, Iwasaki S, Takahashi T. Distinct roles of Kv1 and Kv3 potassium channels at the calyx of Held presynaptic terminal. J Neurosci. 2003; 23:10445–10453. [PubMed: 14614103]

Johnson SL, Franz C, Kuhn S, Furness DN, Ruttiger L, Munkner S, Rivolta MN, Seward EP, Herschman HR, Engel J, Knipper M, Marcotti W. Synaptotagmin IV determines the linear Ca2+ dependence of vesicle fusion at auditory ribbon synapses. Nat Neurosci. 2010; 13:45–52. [PubMed: 20010821]

Jones MV, Westbrook GL. The impact of receptor desensitization on fast synaptic transmission. Trends Neurosci. 1996; 19:96–101. [PubMed: 9054063]

Katsuki Y, Sumi T, Uchiyama H, Watanabe T. Electric responses of auditory neurons in cat to sound stimulation. J Neurophysiol. 1958; 21:569–588. [PubMed: 13599048]

Keen EC, Hudspeth AJ. Transfer characteristics of the hair cell's afferent synapse. Proc Natl Acad Sci U S A. 2006; 103:5537–5542. [PubMed: 16567618]

Kevetter GA. Pattern of selected calcium-binding proteins in the vestibular nuclear complex of two rodent species. J Comp Neurol. 1996; 365:575–584. [PubMed: 8742303]

Kim M-H, Li G-L, von Gersdorff H. Single Ca2+ channels and exocytosis at sensory synapses. J. Physiol. 2013; 591:3167–3178. [PubMed: 23459757]

Klug A, Borst JG, Carlson BA, Kopp-Scheinpflug C, Klyachko VA, Xu-Friedman MA. How do short-term changes at synapses fine-tune information processing? J Neurosci. 2012; 32:14058–14063. [PubMed: 23055473]

Klyachko VA, Stevens CF. Temperature-dependent shift of balance among the components of short-term plasticity in hippocampal synapses. J. Neurosci. 2006; 26:6945–6957. [PubMed: 16807324]

Kochubey O, Han Y, Schneggenburger R. Developmental regulation of the intracellular Ca2+ sensitivity of vesicle fusion and Ca2+-secretion coupling at the rat calyx of Held. J. Physiol. 2009; 587:3009–3023. [PubMed: 19403608]

Kolkman KE, McElvain LE, du Lac S. Diverse precerebellar neurons share similar intrinsic excitability. J Neurosci. 2011; 31:16665–16674. [PubMed: 22090493]

Korn H, Faber DS, Burnod Y, Triller A. Regulation of efficacy at central synapses. J Neurosci. 1984; 4:125–130. [PubMed: 6198489]

Kraushaar U, Jonas P. Efficacy and stability of quantal GABA release at a hippocampal interneuron-principal neuron synapse. J. Neurosci. 2000; 20:5594–5607. [PubMed: 10908596]

Larson CR, Finocchio DV, Smith A, Luschei ES. Jaw muscle afferent firing during an isotonic jaw-positioning task in the monkey. J. Neurophysiol. 1983; 50:61–73. [PubMed: 6223990]

Lasker DM, Han GC, Park HJ, Minor LB. Rotational responses of vestibular-nerve afferents innervating the semicircular canals in the C57BL/6 mouse. J Assoc Res Otolaryngol. 2008; 9:334–348. [PubMed: 18473139]

Lisberger SG, Fuchs AF. Role of primate flocculus during rapid behavioral modification of vestibuloocular reflex. I. Purkinje cell activity during visually guided horizontal smooth-pursuit eye movements and passive head rotation. J. Neurophysiol. 1978a; 41:733–763. [PubMed: 96225]

Lisberger SG, Fuchs AF. Role of primate flocculus during rapid behavioral modification of vestibuloocular reflex. II. Mossy fiber firing patterns during horizontal head rotation and eye movement. J. Neurophysiol. 1978b; 41:764–777. [PubMed: 96226]

Lorteije JA, Rusu SI, Kushmerick C, Borst JG. Reliability and precision of the mouse calyx of Held synapse. J Neurosci. 2009; 29:13770–13784. [PubMed: 19889989]

Matveev V, Bertram R, Sherman A. Calcium cooperativity of exocytosis as a measure of Ca^{2}+ channel domain overlap. Brain Res. 2011; 1398:126–138. [PubMed: 21621748]

McCandless CH, Balaban CD. Parabrachial nucleus neuronal responses to off-vertical axis rotation in macaques. Exp Brain Res. 2010; 202:271–290. [PubMed: 20039027]

McElvain LE, Bagnall MW, Sakatos A, du Lac S. Bidirectional plasticity gated by hyperpolarization controls the gain of postsynaptic firing responses at central vestibular nerve synapses. Neuron. 2010; 68:763–775. [PubMed: 21092864]

Meng H, May PJ, Dickman JD, Angelaki DE. Vestibular signals in primate thalamus: properties and origins. J Neurosci. 2007; 27:13590–13602. [PubMed: 18077671]

Menzies JRW, Porrill J, Dutia M, Dean P. Synaptic plasticity in medial vestibular nucleus neurons: Comparison with computational requirements of VOR adaptation. PLoS One. 2010:5.

Meyer AC, Neher E, Schneggenburger R. Estimation of quantal size and number of functional active zones at the calyx of held synapse by nonstationary EPSC variance analysis. J Neurosci. 2001; 21:7889–7900. [PubMed: 11588162]

Mintz IM, Sabatini BL, Regehr WG. Calcium control of transmitter release at a cerebellar synapse. Neuron. 1995; 15:675–688. [PubMed: 7546746]

Mosbacher J, Schoepfer R, Monyer H, Burnashev N, Seeburg PH, Ruppersberg JP. A molecular determinant for submillisecond desensitization in glutamate receptors. Science. 1994; 266:1059–1062. [PubMed: 7973663]

Murphy GJ, Glickfeld LL, Balsen Z, Isaacson JS. Sensory neuron signaling to the brain: properties of transmitter release from olfactory nerve terminals. J. Neurosci. 2004; 24:3023–3030. [PubMed: 15044541]

Neher E. What is Rate-Limiting during Sustained Synaptic Activity: Vesicle Supply or the Availability of Release Sites. Front Synaptic Neurosci. 2010; 2:144. [PubMed: 21423530]

Nicoll RA, Tomita S, Bredt DS. Auxiliary subunits assist AMPA-type glutamate receptors. Science. 2006; 311:1253–1256. [PubMed: 16513974]

Partin KM, Fleck MW, Mayer ML. AMPA receptor flip/flop mutants affecting deactivation, desensitization, and modulation by cyclothiazide, aniracetam, and thiocyanate. J Neurosci. 1996; 16:6634–6647. [PubMed: 8824304]

Pfister JP, Dayan P, Lengyel M. Synapses with short-term plasticity are optimal estimators of presynaptic membrane potentials. Nat Neurosci. 2010; 13:1271–1275. [PubMed: 20852625]

Priel A, Kolleker A, Ayalon G, Gillor M, Osten P, Stern-Bach Y. Stargazin reduces desensitization and slows deactivation of the AMPA-type glutamate receptors. J Neurosci. 2005; 25:2682–2686. [PubMed: 15758178]

Raymond J, Dechesne CJ, Desmadryl G, Dememes D. Different calcium-binding proteins identify subpopulations of vestibular ganglion neurons in the rat. Acta Otolaryngol Suppl. 1993; 503:114–118. [PubMed: 8385864]

Ritzau-Jost A, Delvendahl I, Rings A, Byczkowicz N, Harada H, Shigemoto R, Hirrlinger J, Eilers J, Hallermann S. Ultrafast Action Potentials Mediate Kilohertz Signaling at a Central Synapse. Neuron. 84:152–163. [PubMed: 25220814]

Robinson DA. The use of control systems analysis in the neurophysiology of eye movements. Annu Rev Neurosci. 1981; 4:463–503. [PubMed: 7013640]

Rollenhagen A, Lubke JH. The morphology of excitatory central synapses: from structure to function. Cell Tissue Res. 2006; 326:221–237. [PubMed: 16932936]

Rudy B, McBain CJ. Kv3 channels: voltage-gated K+ channels designed for high-frequency repetitive firing. Trends Neurosci. 2001; 24:517–526. [PubMed: 11506885]

Sabatini BL, Regehr WG. Control of neurotransmitter release by presynaptic waveform at the granule cell to Purkinje cell synapse. J Neurosci. 1997; 17:3425–3435. [PubMed: 9133368]

Sadeghi SG, Minor LB, Cullen KE. Neural Correlates of Sensory Substitution in Vestibular Pathways following Complete Vestibular Loss. J. Neurosci. 2012; 32:14685–14695. [PubMed: 23077054]

Sato F, Sasaki H. Morphological correlations between spontaneously discharging primary vestibular afferents and vestibular nucleus neurons in the cat. J Comp Neurol. 1993; 333:554–566. [PubMed: 8370817]

Saviane C, Silver RA. Fast vesicle reloading and a large pool sustain high bandwidth transmission at a central synapse. Nature. 2006a; 439:983–987. [PubMed: 16496000]

Saviane C, Silver RA. Errors in the estimation of the variance: implications for multiple-probability fluctuation analysis. J Neurosci Methods. 2006b; 153:250–260. [PubMed: 16376992]

Saviane C, Silver RA. Estimation of quantal parameters with multiple- probability fluctuation analysis. Methods Mol Biol. 2007; 403:303–317. [PubMed: 18828002]

Scarduzio M, Panichi R, Pettorossi VE, Grassi S. The repetition timing of high frequency afferent stimulation drives the bidirectional plasticity at central synapses in the rat medial vestibular nuclei. Neuroscience. 2012; 223:1–11. [PubMed: 22863673]

Schluter OM, Xu W, Malenka RC. Alternative N-terminal domains of PSD-95 and SAP97 govern activity-dependent regulation of synaptic AMPA receptor function. Neuron. 2006; 51:99–111. [PubMed: 16815335]

Schneggenburger R, Meyer AC, Neher E. Released fraction and total size of a pool of immediately available transmitter quanta at a calyx synapse. Neuron. 1999; 23:399–409. [PubMed: 10399944]

Schneggenburger R, Neher E. Intracellular calcium dependence of transmitter release rates at a fast central synapse. Nature. 2000; 406:889–893. [PubMed: 10972290]

Schneggenburger R, Neher E. Presynaptic calcium and control of vesicle fusion. Curr Opin Neurobiol. 2005; 15:266–274. [PubMed: 15919191]

Shimamoto K, Lebrun B, Yasuda-Kamatani Y, Sakaitani M, Shigeri Y, Yumoto N, Nakajima T. DL-threo-beta-benzyloxyaspartate, a potent blocker of excitatory amino acid transporters. Mol Pharmacol. 1998; 53:195–201. [PubMed: 9463476]

Shimazu H, Precht W. Tonic and kinetic responses of cat's vestibular neurons to horizontal angular acceleration. J Neurophysiol. 1965; 28:991–1013. [PubMed: 5295930]

Silver RA. Estimation of nonuniform quantal parameters with multiple-probability fluctuation analysis: theory, application and limitations. J Neurosci Methods. 2003; 130:127–141. [PubMed: 14667542]

Taschenberger H, von Gersdorff H. Fine-tuning an auditory synapse for speed and fidelity: developmental changes in presynaptic waveform, EPSC kinetics, and synaptic plasticity. J. Neurosci. 2000; 20:9162–9173. [PubMed: 11124994]

Telgkamp P, Padgett DE, Ledoux VA, Woolley CS, Raman IM. Maintenance of high-frequency transmission at purkinje to cerebellar nuclear synapses by spillover from boutons with multiple release sites. Neuron. 2004; 41:113–126. [PubMed: 14715139]

Thanawala MS, Regehr WG. Presynaptic calcium influx controls neurotransmitter release in part by regulating the effective size of the readily releasable pool. J. Neurosci. 2013; 33:4625–4633. [PubMed: 23486937]

Varela JA, Sen K, Gibson J, Fost J, Abbott LF, Nelson SB. A quantitative description of short-term plasticity at excitatory synapses in layer 2/3 of rat primary visual cortex. J Neurosci. 1997; 17:7926–7940. [PubMed: 9315911]

von Gersdorff H, Borst JG. Short-term plasticity at the calyx of held. Nat Rev Neurosci. 2002; 3:53–64. [PubMed: 11823805]

Wong AY, Graham BP, Billups B, Forsythe ID. Distinguishing between presynaptic and postsynaptic mechanisms of short-term depression during action potential trains. J Neurosci. 2003; 23:4868–4877. [PubMed: 12832509]

Wu LG, Borst JG. The reduced release probability of releasable vesicles during recovery from short-term synaptic depression. Neuron. 1999; 23:821–832. [PubMed: 10482247]

Xu-Friedman MA, Regehr WG. Structural contributions to short-term synaptic plasticity. Physiol Rev. 2004; 84:69–85. [PubMed: 14715911]

Zucker RS, Regehr WG. Short-term synaptic plasticity. Annu Rev Physiol. 2002; 64:355–405. [PubMed: 11826273]

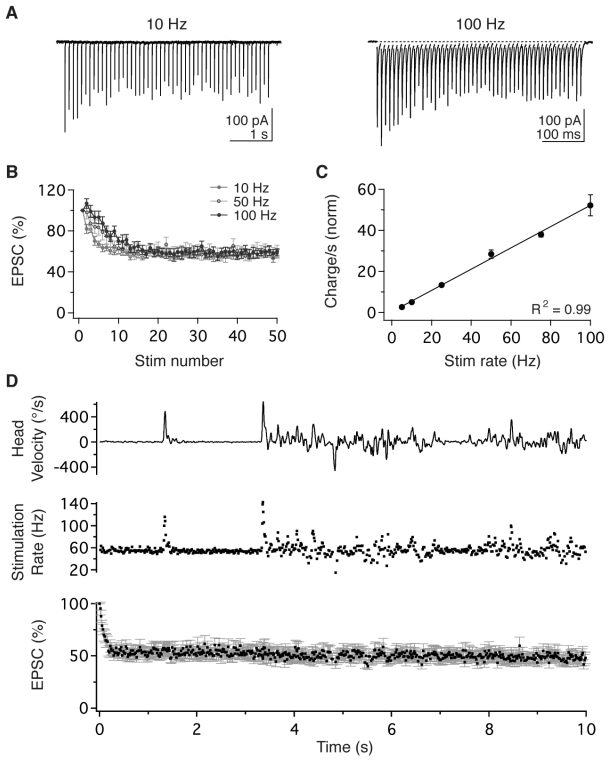

Figure 1.

Sustained, rate-invariant transmission enables vestibular nerve synapses to mediate broadband linear signaling. (A) EPSCs in a vestibular nucleus neuron evoked by vestibular nerve stimulation at 10 Hz (left) and 100 Hz (right). (B) Population data obtained during stimulation at 10, 50, and 100 Hz show that EPSC amplitude depressed to a steady-state level that was independent of stimulus rate (n=11). (C) Steady-state charge transfer increased linearly with stimulation rate. Data show steady-state charge transfer per second normalized to the charge transfer of the initial EPSC (n=11). (D) EPSC amplitude remained constant during physiological variations in vestibular nerve activity. Head motion of a freely behaving mouse (top) was used to generate a naturalistic afferent firing pattern (middle). Naturalistic stimulation of the vestibular nerve evoked EPSCs that depressed rapidly to a sustained steady-state level (bottom, n=10). Error bars = SEM for all panels and in subsequent figures.

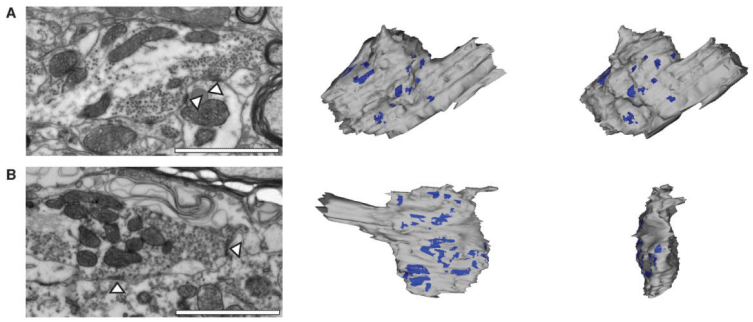

Figure 2.

Central vestibular nerve synaptic transmission is mediated by large presynaptic boutons endowed with multiple release sites. (A, left) Electron microscopic image of an axodendritic vestibular nerve bouton showing two active zones (arrowheads) apposed to a vestibular nucleus neuron dendrite; scale bar = 1 μM. (A, middle) Three dimensional reconstruction of the bouton and (right) its 55 degree rotation demonstrate multiple active zones. (B, left) Electron microscopic image of an axosomatic vestibular nerve terminal bouton showing two active zones (arrowheads) apposed to a somata; scale bar = 1 μM. (B, middle) Reconstruction of the bouton showing multiple active zones apposed to the postsynaptic somata. (right) 90 degree rotation of axosomatic bouton; scale bar for reconstructions = 2 μM.

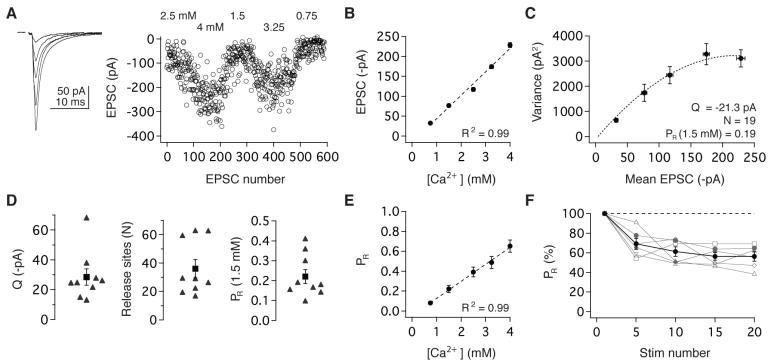

Figure 3.

Vestibular nerve synapses exhibit a linear dependence on calcium and comprise multiple low-probability release sites. (A) Average EPSC waveforms (left) and peak amplitudes (right) evoked under different extracellular Ca2+ concentrations. (B) Peak EPSC amplitude scaled linearly with Ca2+ concentration from 0.75 to 4 mM. (C) Quantal properties were determined from the corresponding variance-mean plot and fit from a multinomial model. Variance error estimated using h-statistics (see Experimental Procedures). (D) MPFA estimates of Q_P, N, and P_R for nine synapses. Across the population, P_R was intermediate-low under physiological conditions (1.5 mM Ca2+) and (E) increased linearly with extracellular Ca2+. (F) P_R decreased in response to repeated vestibular nerve activity. CV analyses estimated P_R during a 10 Hz stimulus train in 1.5 mM Ca2+; individual synapses (grey) and the population (black), binned every 5 pulses (n = 6).

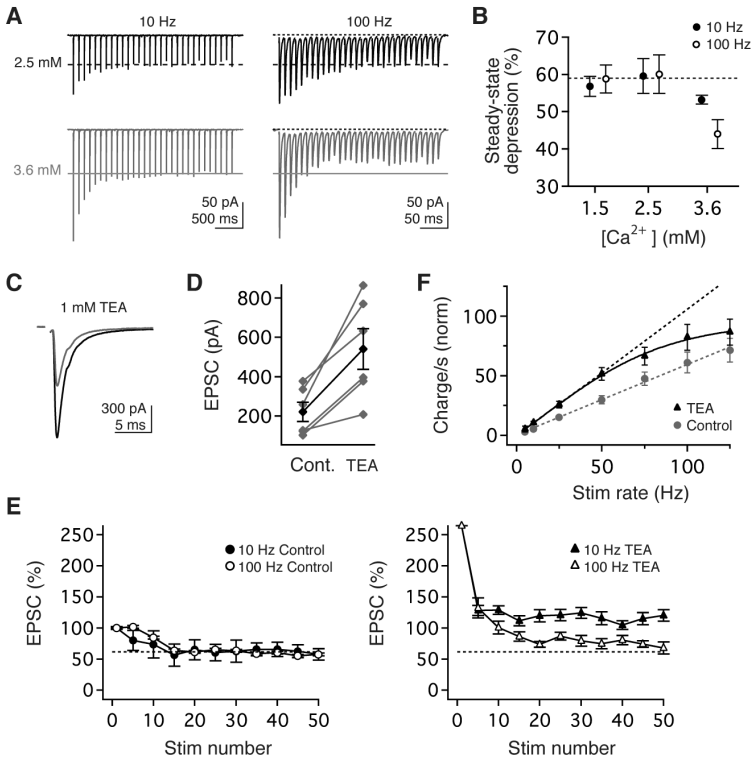

Figure 4.

Synaptic linearity requires low release probability and rapid repolarization of presynaptic action potentials. (A) Example EPSCs evoked in 2.5mM (top, black) and 3.6 mM (bottom, grey) Ca2+ by stimulus trains at 10 Hz (left) and 100 Hz (right). (B) The magnitude of steady-state transmission did not depend on stimulus rate or Ca2+ in 1.5 or 2.5 mM Ca, but depression was rate-dependent in 3.6 mM Ca2+. (C, D) Pharmacological blockade of fast presynaptic K currents with 1 mM TEA markedly increased peak EPSC amplitude. (E, left) Prior to TEA application, the magnitude of short-term depression was comparable for EPSCs evoked by10 Hz or 100 Hz stimuli. (E) Blockade of Kv3 and BK currents enhanced the magnitude of steady-state transmission and compromised rate-independence. (F) Normalized steady-state charge transfer per second before (circles, grey) and during TEA application (triangles, black), normalized to control $EPSC_1$. Dashed lines are the linear extrapolations of data ≤ 50 Hz.

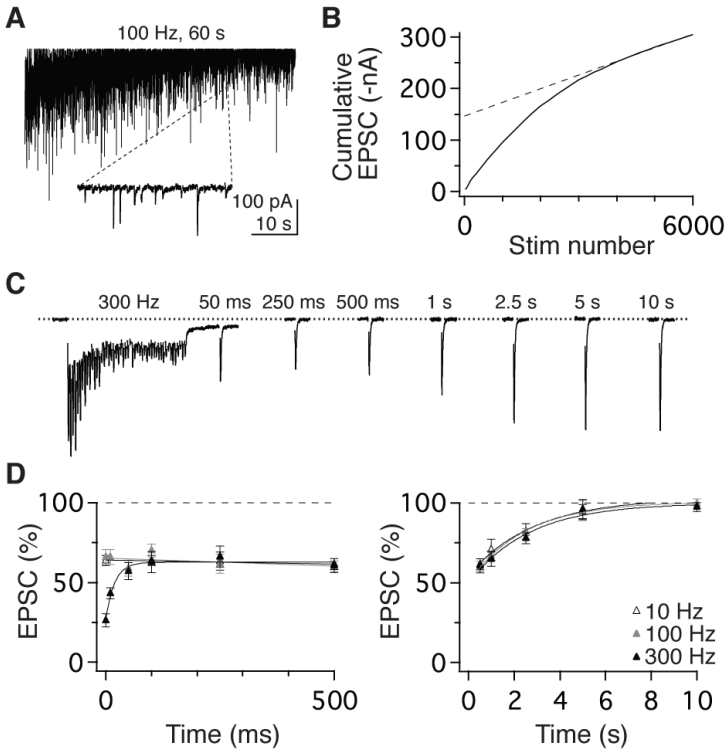

Figure 5.

Rapid vesicle dynamics and slow recovery from steady-state depression. (A) EPSCs evoked by 6,000 stimuli delivered at 100 Hz. Inset shows expanded 220- ms epoch demonstrating occasional failures in transmission after 4,000 stimuli. (B) Linear fit to the last 20 s (dashed line) of the corresponding cumulative EPSC plot (solid line) used to calculate kinetics of vesicle pool reloading. (C) Stimulation at 300 Hz evoked enhanced short-term depression. EPSC amplitude rapidly recovered to an intermediate, steady-state level that was sustained for 500 ms prior to slowly recovering to baseline. (D, left) Recovery timecourse of EPSCs following 50-pulse stimulus trains delivered at 10, 100, and 300 Hz (open, grey, and filled symbols, respectively). Depression from the 300 Hz stimulus recovered rapidly (τ = 22 ms) to the steady-state level evoked at 10 and 100 Hz. (D, right) EPSC amplitude recovered slowly from steady-state, to baseline with timecourses that were independent of stimulus rates: τ = 2.9 s (10 Hz), 2.5 s (100 Hz), and 2.7 s (300 Hz).

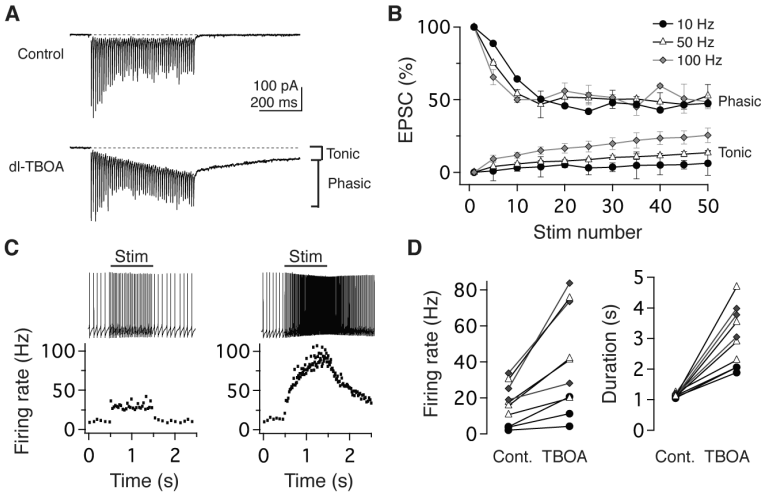

Figure 6.

The temporal fidelity of postsynaptic responses requires active glutamate uptake. (A) Example EPSCs evoked by 100 Hz stimulation in ACSF (top) and following the addition of the 200 μM dl-TBOA (bottom), which resulted in the accumulation of a tonic current in addition to phasic EPSC responses. (B) In dl- TBOA, phasic EPSC responses remained rate-invariant in response to train stimulation at 10, 50, and 100 Hz, however the tonic current progressively increased with rate (n=4). EPSCs normalized to $EPSC_1$ peak amplitude. (C) Example evoked postsynaptic firing responses to a 1-s, 50-Hz train (left) and following dl-TBOA application (right). The instantaneous firing rate (below) demonstrates a step-like response under control conditions and an enhanced, long-lasting response in dl- TBOA. (D) The population effects of blocking glutamate transporters on the firing rate (left) and duration (right) of postsynaptic responses to 1-s stimuli.

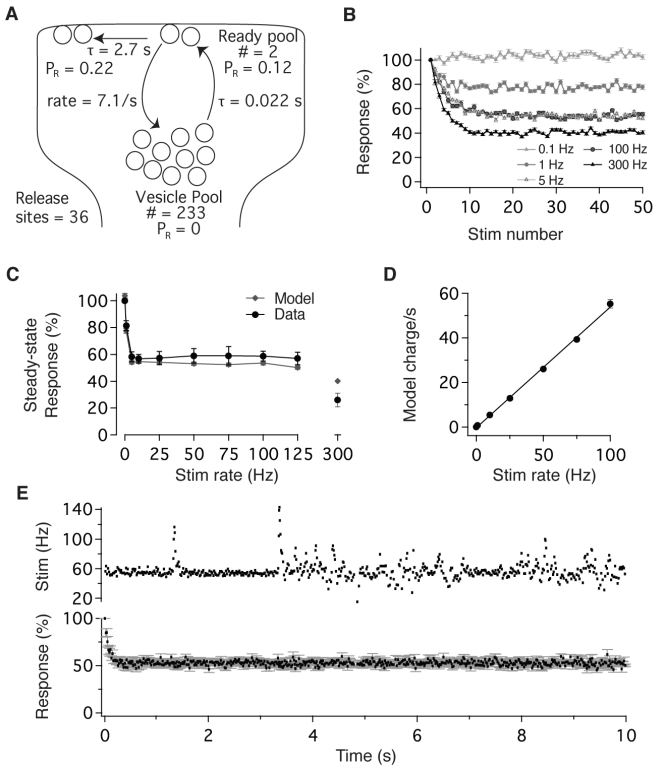

Figure 7.

A simple model constrained by physiological analyses accounts for short- term plasticity and broadband linearity. (A) Schematic of vestibular nerve synapse model based on experimentally-determined measurements. (B) Model response to stimulus trains delivered at 0.1, 1, 5, 100, and 300 Hz. (C) Dependence of steady- state synaptic efficacy ($EPSC_{30\text{-}50}/EPSC_1$) on stimulus rate, determined experimentally (black) and with the model (grey). (D) Modeled steady-state charge transfer scaled linearly with stimulus rate across the physiological range, congruent with experimental results (compare with Figure 1C). (E) Modeled EPSC amplitude remained constant during naturalistic variations in vestibular nerve activity. Stimulation with naturalistic patterns (top) evokes model EPSCs that depressed rapidly to a steady-state level that was independent of stimulus rate (below, n=10 synapses simulated). Error bars = SEM for all panels.

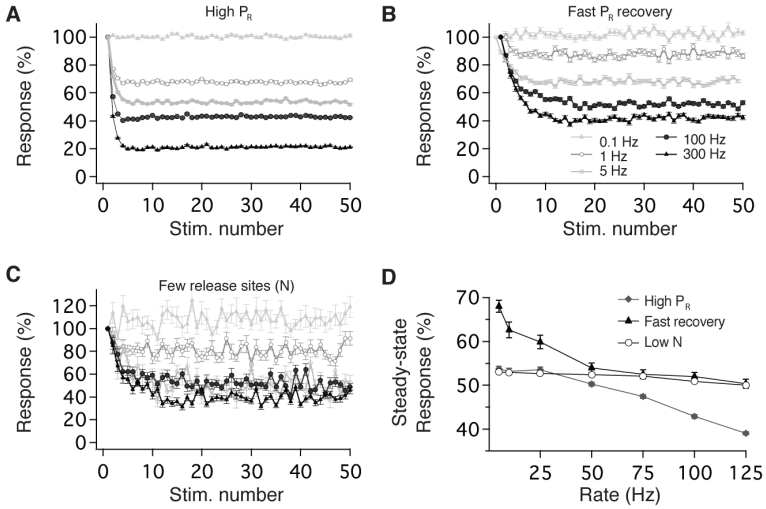

Figure 8.

The range of rate-invariant depression is determined by specific synaptic properties. Panels show perturbations of model parameters that differentially influence short-term depression evoked by stimulus trains at 0.1, 1, 5, 100, and 300 Hz. (A) Increasing initial P_R from 0.22 to 0.64 results in synaptic depression whose magnitude increases with stimulus rate. (B) Accelerating the timecourse of recovery from the P_R depression resulted in rate-dependent transmission by limiting depression at low physiological rates. (C) Reducing the number of release sites from 36 to 5 increased response variability without affecting rate-invariance. (D) Summary of perturbation effects on the rate-invariance of synaptic transmission. Steady-state outputs ($EPSC_{30\text{-}50}$) plotted vs. stimulation rate for models with high P_R (grey diamonds), rapid recovery from steady-state depression (black triangles) and fewer release sites (Low N:open circles). Model results are the average of 200 repetitions, except for the Low N results in (D) which are the average of 5000 repetitions.